BMC Cancer

RESEARCH Open Access

^{18}F-FDG PET/CT-based intratumoral and peritumoral radiomics combining ensemble learning for prognosis prediction in hepatocellular carcinoma: a multi-center study

Chunxiao Sui[1,2†], Kun Chen[3†], Enci Ding[4], Rui Tan[5], Yue Li[4], Jie Shen[4*], Wengui Xu[1,2*] and Xiaofeng Li[1,2*]

Abstract

Background Radiomic models combining intratumoral with peritumoral features are potentially beneficial to enhance the predictive performance. This study aimed to identify the optimal ^{18}F-FDG PET/CT-derived radiomic models for prediction of prognosis in hepatocellular carcinoma (HCC).

Methods A total of 135 HCC patients from two institutions were retrospectively included. Four peritumoral regions were defined by dilating tumor region with thicknesses of 2 mm, 4 mm, 6 mm, and 8 mm, respectively. Based on segmentation of intratumoral, peritumoral and integrated volume of interest (VOI), corresponding radiomic features were extracted respectively. After feature selection, a total of 15 intratumoral radiomic models were constructed based on five ensemble learning algorithms and radiomic features from three image modalities. Then, the optimal combination of ensemble learning algorithms and image modality in the intratumoral models was selected to develop subsequent peritumoral radiomic models and integrated radiomic models. Finally, a nomogram was developed incorporating the optimal radiomic model with clinical independent predictors to achieve an intuitive representation of the prediction model.

Results Among the intratumoral radiomic models, the one which combined PET/CT-based radiomic features with SVM classifier outperformed other models. With the addition of peritumoral information, the integrated model based on an integration of intratumoral and 2 mm-peritumoral VOI, was finally approved as the optimal radiomic model with a mean AUC of 0.831 in the internal validation, and a highest AUC of 0.839 (95%CI:0.718–0.960) in the external

†Chunxiao Sui and Kun Chen contributed equally to this work.

*Correspondence:
Jie Shen
shenjie_vip@126.com
Wengui Xu
wenguixy@yeah.net
Xiaofeng Li
xli03@tmu.edu.cn

Full list of author information is available at the end of the article

© The Author(s) 2025. **Open Access** This article is licensed under a Creative Commons Attribution-NonCommercial-NoDerivatives 4.0 International License, which permits any non-commercial use, sharing, distribution and reproduction in any medium or format, as long as you give appropriate credit to the original author(s) and the source, provide a link to the Creative Commons licence, and indicate if you modified the licensed material. You do not have permission under this licence to share adapted material derived from this article or parts of it. The images or other third party material in this article are included in the article's Creative Commons licence, unless indicated otherwise in a credit line to the material. If material is not included in the article's Creative Commons licence and your intended use is not permitted by statutory regulation or exceeds the permitted use, you will need to obtain permission directly from the copyright holder. To view a copy of this licence, visit http://creativecommons.org/licenses/by-nc-nd/4.0/.

test. Furthermore, a nomogram incorporating the optimal radiomic model with HBV infection and TNM status, was able to predict the prognosis for HCC with an AUC of 0.889 (95%CI: 0.799–0.979).

Conclusions The integrated intratumoral and peritumoral radiomic model, especially for a 2 mm peritumoral region, was verified as the optimal radiomic model to predict the overall survival of HCC. Furthermore, combination of integrated radiomic model with significant clinical parameter contributed to further enhance the prediction efficacy.

Trial registration This study was a retrospective study, so it was free from registration.

Keywords ^{18}F-FDG PET/CT, Radiomics, Peritumoral, HCC, Prognosis

Background

Hepatocellular carcinoma (HCC) stands as the predominant primary liver malignancy, ranking third in cancer-related mortality [1–3]. Chronic liver diseases like hepatitis virus infection, severe fibrosis and/or cirrhosis constitute major risk factors for HCC[4, 5]. Due to the lack of classical symptom, it was difficult to achieve early diagnosis and administrate timely and effective therapy for HCC[6, 7]. Consequently, the prognosis for HCC is still not satisfactory. To improve the clinical prospect for HCC, potentially prognostic factors are urgently needed to guide clinical stating and treatment decision-making. Multiple staging methods, such as the Barcelona Clinic Liver Cancer staging system (BCLC), the Cancer of the Liver Italian Program (CLIP) and the Okuda criteria, are already commonly applied in clinical practice for HCC based on clinical and biochemical information[8, 9]. Though these staging systems are helpful to prognosis prediction for HCC, their predictive performance are limited and needed to be improved. An effective and reliable imaging index is a promising substitute to predict clinical outcome for HCC, which is also a focus in related field.

^{18}F-Fluorodeoxyglucose positron emission tomography/computed tomography (^{18}F-FDG PET/CT) imaging is capable of providing both anatomical information from CT images and metabolic information from PET images, thus it is widely used in diagnosis, staging and response evaluation for multiple types of malignant tumors [10–13]. Especially for survival analysis, multiple traditional PET metabolic parameters, including maximum standardized uptake value (SUVmax), metabolic tumor volume (MTV), total lesion glycolysis (TLG) and tumor liver uptake ratio (TLR), are recognized as promising indicator for clinical outcome in HCC. Han et al. revealed that preoperative SUV was a potential prognostic factor, and a scoring system based on that was thus developed to predict recurrence and survival for HCC after surgical resection [14]. As expected, SUV was proved to be an independent predictor for recurrence-free survival (RFS) and overall survival (OS) in HCC.Though a higher recurrence rate was found in HCC patients with elevated SUVmax by Cho et al., no significant difference was observed between different SUVmax groups in terms of disease-free survival (DFS) and OS [15]. In a word, there is no consensus on the relationship between PET/CT traditional metabolic parameters and clinical outcomes for HCC. A further study is urgently needed to comprehensively evaluate the role of ^{18}F-FDG PET/CT in prognosis prediction for HCC.

Radiomics represents a nascent form of imaging analysis employing a range of data mining algorithms or statistical tools on high-throughput imaging features to extract predictive information and construct prediction models [16–19]. Currently, radiomics based on computed tomography (CT) and/or magnetic resonance imaging (MRI) images are proved to be potentially effective predictors for recurrence estimation and prognosis prediction in HCC with a higher accuracy compared to single clinicopathologic index, which are expected to be translationally applied in clinical practice in future [20–22]. Whereas, to the best of our knowledge, limited efforts are made to assess prognosis for HCC using PET/CT derived radiomics[4, 5]. Therefore, we deduced that PET/CT radiomic analysis would offer comparable or incremental value in predicting prognosis and clinical outcomes compared to single-modal imaging models.

Though peritumoral region was previously reported as a superior predictor for recurrence and metastasis in comparison with intratumoral region, radiomics predominantly focused on the intratumoral region alone, neglecting the information from peritumoral region [23–26]. Given the substantial nature of liver, the peritumoral region in HCC was expected to harbor crucially complementary information closely associated with tumor characteristics. The average range of peritumoral regions was reported from 1.5 to 8 mm beyond the apparent borders of intratumoral regions themselves in microscopic field in previous studies [27–29]. Nevertheless, a systematical investigation for the optimal size of the peritumoral region for prognosis in HCC is lacking by now.

In this study, a comprehensive radiomic analysis based on ^{18}F-FDG PET/CT were performed to identify the optimal radiomic model for prediction of prognosis in HCC, including intratumoral, peritumoral and integrated radiomics. Additionally, a total of four patterns of peritumoral region sizes were employed to specialize the role of peritumoral radiomics in enhancing the prediction

performance. Finally, a nomogram combining the optimal PET/CT derived radiomic model with significant clinical information was developed to evaluate the potential translational application of this combined model.

Materials and methods

Study population

A total of 681 pathologically diagnosed HCC patients who underwent ^{18}F-FDG PET/CT imaging within 2 weeks before treatment from two institutions were retrospectively reviewed in our study. The inclusion and exclusion criteria for this investigation are shown in Fig. 1. As shown, 84 cases from Tianjin First Central Hospital and 51 cases from Tianjin Medical University Cancer Institute and Hospital were ultimately included as a training/internal validation cohort and an external testing cohort, respectively. This study was approved by our institutional ethics committee, and written informed consent was waived in the present investigation. All procedures involving human participants adhered to the principles outlined in the 1964 Helsinki Declaration and its subsequent amendments.

Follow-up

Continuous follow-up was performed for all included HCC patients at an interval of 3 to 6 months after the initiation of treatment, until the date of death, which was defined as OS. The median OS for all included HCC patients from two institutions was determined to be 15 months, enabling the classification of patients into categories of low OS and high OS.

Image acquisition

For ^{18}F-FDG PET/CT imaging, HCC patients were instructed to fast for at least 6 h and maintain their blood glucose levels < 11.1 mmol/L. Then, each patient received an intravenous injection of 3.7–5.55 MBq/kg (0.1–0.15 mCi/kg) of ^{18}F-FDG. Following the injection, patients were advised to rest in a dimly lit and quiet environment for approximately 60 min. The scanning range extended from the skull base to the distal femur. The detailed device scanning parameters was referred to the Supplementary Material. All images were independently reviewed by two experienced nuclear experts, and any disagreement was resolved by consensus.

PET metabolic and volumetric parameters calculation

The traditional metabolic and volumetric parameters based on PET images were calculated by using the volume-of-interest (VOI) technique, which was determined using an isocontour threshold method based on SUV using a commercial software (PET VCAR; GE Healthcare, USA) in GE Advantage Workstation 4.6 (AW 4.6). All three conventional SUV parameters (SUVmax,

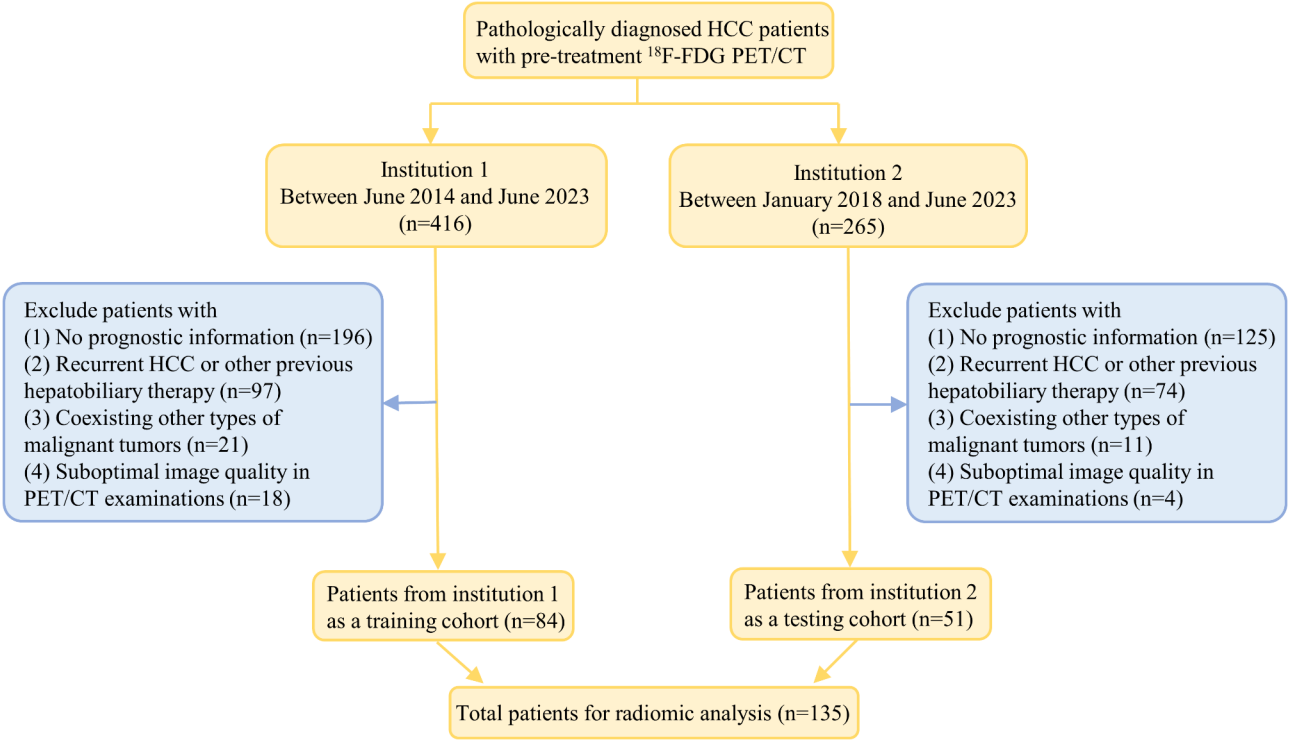

Fig. 1 The enrollment of the candidates in the study was flowcharted. *HCC*: hepatocellular carcinoma; *^{18}F-FDG PET/CT*: ^{18}F-Fluorodeoxyglucose positron emission tomography/computed tomography

SUVmean and SUVpeak) based on body weight and SUV normalized to lean body mass (SUL) were calculated automatically. The metabolic tumor volume (MTV) was a volumetric measurement of a lesion demonstrating markedly elevated ^{18}F-FDG uptake, above a threshold SUV of 2.5. Total lesion glycolysis (TLG) was calculated by multiplying the MTV with SUVmean. The tumor-to-mediastinum ratio (TMR) was the ratio of SUVmax in tumor to SUVmean in mediastinum.

Radiomics based on PET/CT

The workflow of radiomics in the present investigation is drawn in Fig. 2. For the preprocessing, the acquired PET and CT images were resampled to a volume of $1 \times 1 \times 1$ mm to standardize the voxel spacing. Then, the PET images were spatially aligned with corresponding CT images using the rigid registration function within the well-validated Elastix software using 3D Slicer (version: 5.2.2) software. For tumor segmentation, the VOI in the tumoral region (TR) was manually delineated along the border of the tumor lesion slice-by-slice by two nuclear medicine physicians with more than 5-year experience by using the 3D Slicer software, and the masks were shared by the PET and CT images for further analysis. Then, the segmented masks of TR were dilated by 2 mm, 4 mm, 6 mm and 8 mm to obtain four patterns of peritumoral regions (PTR). The tumoral and peritumoral region (TR-PTR) was finally obtained by merging TR with PTR as a whole. The representative PET/CT images and their corresponding VOIs in TR, PTR and TR-PTR were shown in Fig. 3.

Regarding radiomic feature extraction, a total of 4028 radiomic features were extracted based on each VOI using the Pyradiomics module in Python 3.7.0, including 2014 CT-based and 2014 PET-based radiomic features. The detailed information for extracted radiomic features are listed in Figure S1. Additionally, feature normalization was performed by using Z-score to standardize the intensity range. Given that the images originated from different devices, we employed Combat harmonization as a pre-processing step to mitigate the impact of scanner on the results.

For radiomic feature selection, radiomic features with the interclass correlation coefficients (ICC) values ≥ 0.75 were retained [30, 31]. The features with Pearson's correlation coefficients exceeding 0.90 were considered potentially highly related, in which one of the paired features with a lower AUC was excluded. Then, the features with nonzero coefficients after the least absolute shrinkage selection operator (LASSO) regression were selected for further analysis. After radiomic feature selection, a total of 15 intratumoral radiomic models were first constructed based on different combinations of five ensemble learning algorithms, including Logistic Regression

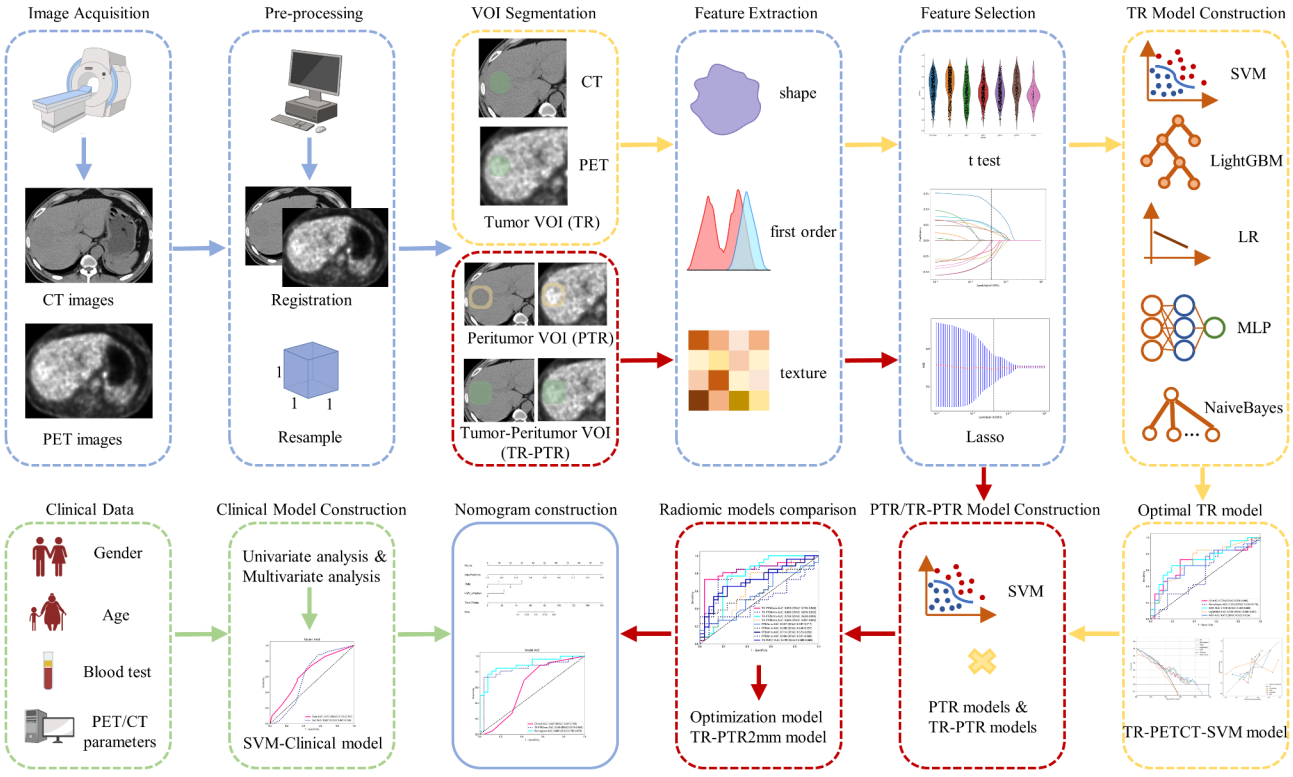

Fig. 2 The overall workflow of the comprehensive radiomic analysis in the study. The process generally consists of image acquisition, image pre-processing, VOI segmentation, feature extraction and selection, radiomic and clinical model development and nomogram construction. *VOI*: volume of interest

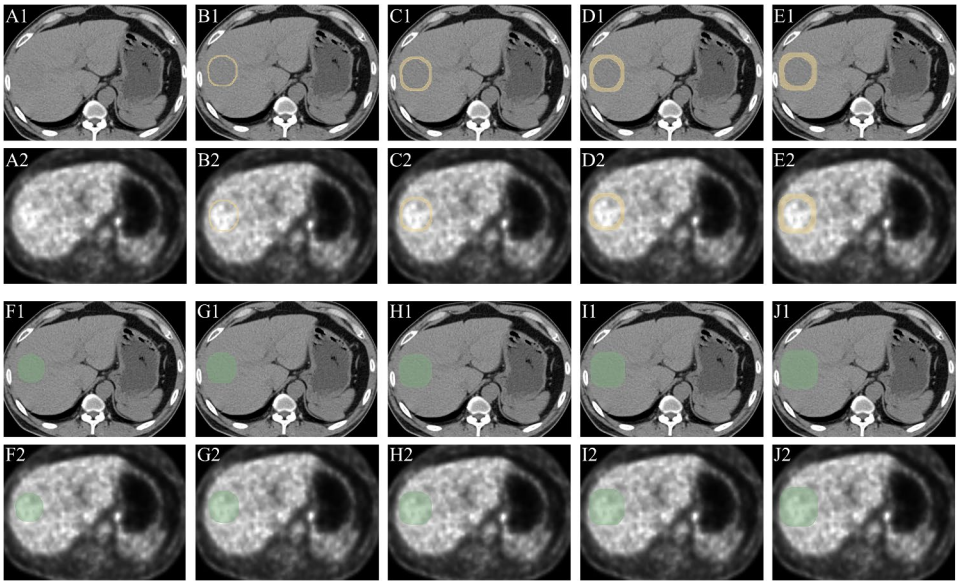

Fig. 3 The representative PET/CT images and corresponding delineations of VOIs. (**A**) The original CT (upper) and PET (lower) images. The delineations of peritumor regions (PTRs) within a 2 mm (**B**), 4 mm (**C**), 6 mm (**D**), and 8 mm (**E**) thickness to the tumor boundary in CT images (upper) and PET images (lower). (**F**) The delineation of intratumoral region (TR) in CT images (upper) and PET images (lower). The segmentations of integrated intratumoral and peritumoral regions (TR-PTR) based on TR delineation with automatic dilated PTR with thicknesses of 2 mm (**G**), 4 mm (**H**), 6 mm (**I**) 8 mm (**J**) in CT images (upper) and PET images (lower)

(LR), support vector machine (SVM), Light Gradient Boosting Machine (LightGBM), Multilayer Perceptron (MLP) and NaiveBayes (NB), with radiomic features based on three image modalities (PET alone, CT alone and PET/CT). Among the intratumoral radiomic models, the optimal combination of ensemble learning algorithm and image modality was selected to develop subsequent peritumoral radiomic models and integrated radiomic models. Additionally, clinical independent indicators were also integrated with finally selected radiomic model with outperformance to develop a nomogram, which provided a visually intuitive representation of the constructed prediction model.

Statistical analysis

The statistical analysis was conducted by using Python 3.7.0 software. A p value below 0.05 was considered statistically significant. Quantitative data conforming to a normal distribution was presented as mean ± SD. The two independent samples t-test was employed for comparison between the two groups. Qualitative data were compared using either the χ^2 test or Fisher's exact test. For feature selection of clinical information, the univariate logistic regression and stepwise multivariate logistic regression analyses were conducted to identify the independent indicator with a p-value < 0.05, which were selected as predictive clinical parameters to establish clinical machine learning models. Several statistical measures were utilized as the primary outcome to assess the performance of these developed radiomic models, including area under the curve (AUC), sensitivity, specificity, positive predictive value (PPV), and negative predictive value (NPV). The receiver operator characteristic (ROC) curve, calibration curve, and decision curve analysis (DCA) were employed correspondingly. The training cohort was randomly divided into 30% as an internal validation set to ensure the stability of the established model. The procedure was repeated 100 times, with the average results serving as the final prediction result under the model. In addition, an independent external testing cohort from institution 2 was used to verify the performance of the model. Delong's test was utilized to assess the differences in AUCs between different constructed radiomic models.

Results

Patient characteristics and clinical prognostic factors

As listed in Table 1, no significant differences in clinical characteristics between the training and validation cohort are observed, except for TLG. Based on the median OS of 15 months, the included HCC cases were categorized into two groups: Low OS and High OS. To identify the clinical prognostic factor for HCC, the univariate logistic regression and stepwise multivariate logistic regression analyses were conducted. As shown in Table 2, the HBV infection (OR 1.209; 95% CI 1.047–1.397; $p = 0.031$) and TNM (OR 1.084; 95% CI 1.023–1.148; $p = 0.021$) were found to be the independent indicators for prognosis. None of the traditional PET metabolic parameters, including SUVmax, SUVpeak, SUVmean, MTV, TLG,

Table 1 Demographic information and clinical characteristics of patients in the training and external testing cohorts

Characteristics	Training cohort ($n=84$)	Testing cohort ($n=51$)	*P* value
Gender			0.425
Female	16 (19.1%)	7 (13.7%)	
Male	68 (80.9%)	44 (86.3%)	
Age[#]	52.92 ± 9.43	54.33 ± 10.66	0.082
BMI[#]	24.07 ± 3.92	25.12 ± 3.41	0.112
AFP			0.886
≤ 200 ng/mL	27 (32.1%)	17 (33.3%)	
> 200 ng/mL	57 (67.9%)	34 (66.7%)	
ALT			0.740
≤ 50 U/L	57 (67.9%)	36 (70.6%)	
> 50 U/L	27 (32.1%)	15 (29.4%)	
TB			0.195
≤ 19 μmol/L	34 (40.5%)	15 (29.4%)	
> 19 μmol/L	50 (59.5%)	36 (70.6%)	
HBV infection			0.071
Never	59 (70.2%)	28 (54.9%)	
Current or former	25 (29.8%)	23 (45.1%)	
Diameter[&]	6.70 (3.60–9.55)	7.05 (4.13–10.33)	0.452
Location			0.132
right lobe of liver	41 (48.8%)	32 (62.7%)	
left lobe of liver	9 (10.7%)	7 (13.7%)	
both lobes of liver	34 (40.5%)	12 (23.5%)	
TNM			0.081
I	22 (26.2%)	8 (15.7%)	
II	17 (20.2%)	6 (11.8%)	
III	25 (29.8%)	15 (29.4%)	
IV	20 (23.8%)	22 (43.1%)	
SUVmax[&]	7.16 (5.05–11.07)	7.91 (5.95–10.11)	0.270
SUVpeak[&]	5.48 (4.06–8.36)	6.90 (4.72–8.64)	0.067
SUVmean[&]	3.52 (3.07–4.36)	4.11 (3.15–5.53)	0.053
MTV[&]	167.04 (31.62–417.80)	202.50 (45.78-414.25)	0.703
TLG[&]	2844.33 (590.00-13963.78)	909.95 (204.99-1575.38)	**<0.01**
SUL[&]	5.79 (4.03–7.91)	6.60 (4.51–8.32)	0.298
TMR[&]	3.49 (2.34–5.11)	3.97 (3.12–5.55)	0.078

[#]A t-test was used for age and BMI

[&]A Mann-Whitney U test was used for diameter, SUVmax, SUVpeak, SUVmean, MTV, TLG, SUL and TMR

A χ^2 test or Fisher's exact test was used for the rest

BMI: body mass index; *AFP*: Alpha-FetoProtein; *ALT*: alanine transaminase; *TB*: total bilirubin; *HBV*: hepatitis B virus; *SUV*: standardized uptake value; *MTV*: metabolic tumor volume; *TLG*: total lesion glycolysis; *SUL*: SUV normalized to lean body mass; *TMR*: tumor-to-mediastinum SUV ratio

SUL and TMR, exhibited statistical significance in distinguishing Low OS from High OS.

Machine learning models based on intratumoral radiomics

After radiomic feature selection, a total of 7 features, 5 features and 9 features were identified as informative features to construct TR-CT model (Figure S2A), TR-PET model (Figure S2B) and TR-PET/CT model (Figure S2C), respectively. Afterwards, 15 machine learning models were established by combining aforementioned three intratumoral radiomic models with five types of ensemble learning algorithms (LR, SVM, LightGBM, MLP and NB). In the internal validation cohort, SVM exhibited outperformance in prognosis prediction in comparison with the other four classifiers, with a mean AUC of 0.722, 0.730, and 0.742 for TR-CT, TR-PET, and TR-PETCT models, respectively (Fig. 4A-C). For the external testing cohort, the TR-PETCT radiomic models, regardless of the machine learning classifier used, outperformed both TR-CT and TR-PET radiomic models (Fig. 4D-F and Table S1), suggesting the superiority of combined PET/CT radiomics over PET alone and CT alone derived radiomics. Ultimately, the TR-PETCT-SVM radiomic model with an AUC of 0.729 (95%CI: 0.589–0.869) was selected as the optimal intratumoral radiomic model for further analysis.

Machine learning models based on peritumoral radiomics, and integration of intratumoral and peritumoral radiomics

Based on the results obtained above, a combination of PET/CT based radiomics and SVM classifier were used as a strategy to construct the peritumoral radiomic models and integrated intra- and peri-tumoral radiomic models, including 4 PTR models and 4 TR-PTR models, which incorporated the peritumoral-only, and the integrated intra- and peri-tumoral features derived from 4 patterns of different peritumoral region sizes (2 mm, 4 mm, 6 mm, 8 mm), respectively. The radiomic features selected by screening procedure to construct TR-$PTR_{2-8\ mm}$ models and $PTR_{2-8\ mm}$ models were demonstrated in Figure S3. For the internal 100-repetition validation, the TR-PTR2mm and TR-PTR4mm models with a mean AUC of 0.831 and 0.812, were considered as the stabilized prediction models (Fig. 5A). For the external testing cohort, the comprehensive performances of all the constructed TR-PTR_{2mm} models and TR-PTR_{4mm} models are summarized in Table 3, and the corresponding ROC curves are depicted in Fig. 5B. Among them, the TR-PTR_{2mm} model with the highest AUC of 0.839 (95%CI: 0.718–0.960) was regarded as the optimal PET/CT-derived radiomic model for predicting the prognosis of HCC. The results of the Delong test were displayed in Fig. 5C.

Nomogram construction

A nomogram was constructed by incorporating the finally selected optimal TR-PTR_{2mm} model with the two independent clinical predictors (HBV infection and TNM) (Fig. 6A). To evaluate the performance of the nomogram in prognosis prediction for HCC, ROC curve of the nomogram is drawn in comparison with that of clinical model and TR-PTR_{2mm} model in Fig. 6B. As shown, the AUC of the nomogram in the external

Table 2 Univariate analysis and multivariate analysis in included HCC patients

Characteristics	Univariate analysis			Multivariate analysis		
	OR	95%CI	*P* value	OR	95%CI	*P* value
Gender	0.874	0.723–1.057	0.241			
Age	0.996	0.989–1.003	0.302			
BMI	0.997	0.978–1.016	0.805			
AFP	1.011	0.868–1.177	0.904			
ALT	0.971	0.832–1.133	0.756			
TB	1.022	0.886–1.178	0.803			
HBV infection	1.267	1.099–1.461	**0.007****	1.209	1.047–1.397	**0.031***
Diameter	1.009	0.992–1.027	0.374			
Location	1.018	0.939–1.102	0.720			
TNM	1.103	1.043–1.166	**0.005****	1.084	1.023–1.148	**0.021***
SUVmax	1.013	1.000-1.026	0.097			
SUVpeak	1.016	1.000-1.033	0.104			
SUVmean	1.038	0.995–1.082	0.144			
MTV	1.000	1.000–1.000	0.494			
TLG	1.000	1.000–1.000	0.785			
SUL	1.015	1.000-1.031	0.107			
TMR	1.021	1.002–1.041	0.071			

OR: odds ratio; CI: confidence interval

*$p<0.05$, **$p<0.01$

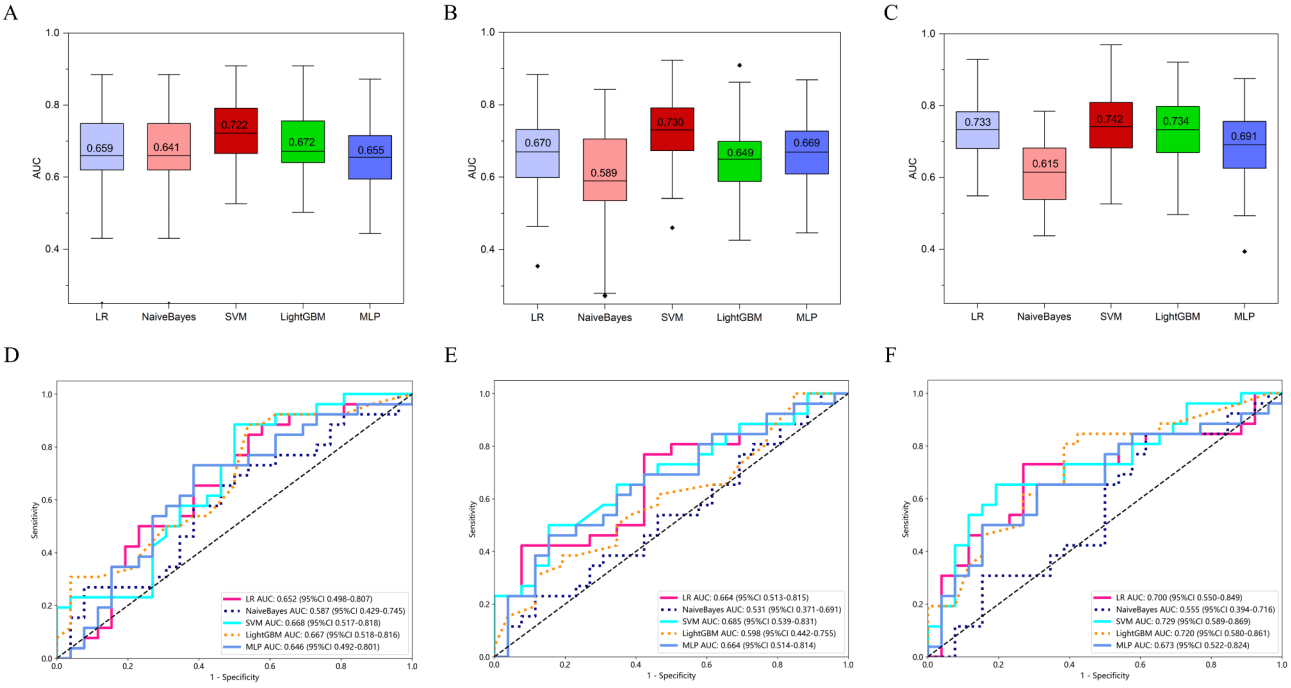

Fig. 4 The stability and performance of the constructed intratumoral radiomic models. The AUCs of internal 100-repetition validation of TR-CT model (**A**), TR-PET model (**B**) and TR-PETCT (**C**) models combined with five machine learning classifiers, including LR, SVM, Light LightGBM, MLP and NB. The horizontal lines in the box plots represented the mean AUC of 100 repetitions. As indicated, SVM was identified to be the optimal classifier with the highest mean AUC of 0.722, 0.730, and 0.742 for TR-CT, TR-PET and TR-PETCT models, respectively. The ROC curves of TR-CT models (**D**), TR-PET models (**E**) and TR-PETCT (**F**) models were also depicted. As shown, the AUCs of TR-PETCT radiomic models in combination with each machine learning classifier was higher than that of TR-CT and TR-PET models. *LR*: logistic Regression; *SVM*: support vector machine; *LightGBM*: light gradient boosting machine; *MLP*: Multilayer Perceptron; *NB*: naivebayes; *ROC*: receiver operator characteristic; *AUC*: area under the curve

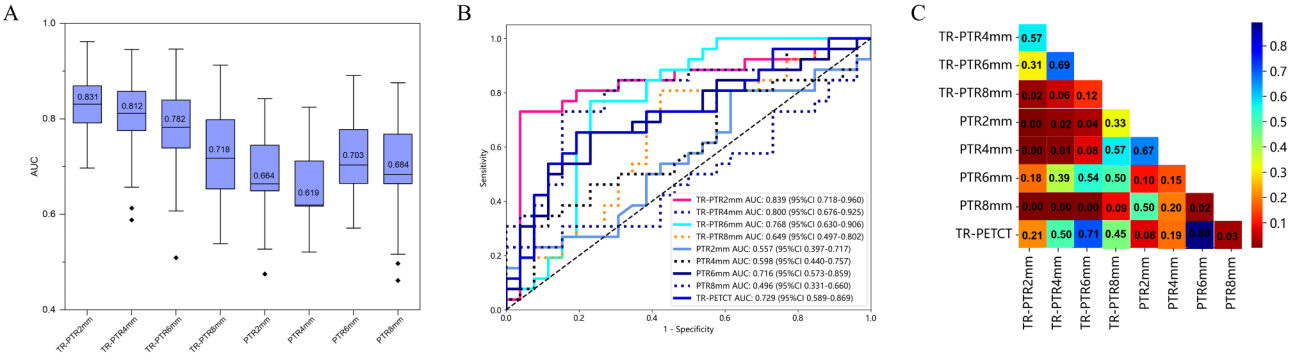

Fig. 5 The stability and performance of the peritumoral radiomic models and the integrated intratumoral and peritumoral radiomic models. (**A**) A total of 4 TR-PTR models and a total of 4 PTR models were constructed based on PET/CT radiomics combined with SVM. The horizontal lines in the box plots represented the mean AUC of 100 repetitions. As indicated, the TR-PTR_{2mm} model was with a highest mean AUC of 0.831. (**B**) ROC curves of TR-$PTR_{2-8\,mm}$ and $PTR_{2-8\,mm}$ models were depicted. As shown, the TR-PTR_{2mm} model with a highest AUC of 0.839 (95%CI: 0.718–0.960) in the independent external cohort was proved to be the optimal model for predicting prognosis of HCC. (**C**) The differences in the prediction performances between the constructed TR-PETCT-SVM model, TR-$PTR_{2-8\,mm}$ models and $PTR_{2-8\,mm}$ models

Table 3 Each evaluation index of intra- and peri- tumoral models in SVM machine learning algorithms of testing cohort

Model Name	AUC (95%CI)	Accuracy	Sensitivity	Specificity	PPV	NPV
TR-PETCT	0.729 (0.5892–0.8694)	0.731	0.654	0.808	0.773	0.700
TR-PTR_{2mm}	0.839 (0.7180–0.9595)	0.846	0.731	0.962	0.950	0.781
TR-PTR_{4mm}	0.800 (0.6757–0.9249)	0.769	0.692	0.846	0.818	0.733
TR-PTR_{6mm}	0.768 (0.6299–0.9056)	0.692	0.577	0.808	0.750	0.656
TR-PTR_{8mm}	0.649 (0.4965–0.8023)	0.596	0.577	0.615	0.600	0.593
PTR_{2mm}	0.557 (0.3967–0.7172)	0.519	0.346	0.692	0.529	0.514
PTR_{4mm}	0.598 (0.4395–0.7572)	0.538	0.538	0.538	0.538	0.538
PTR_{6mm}	0.716 (0.5728–0.8592)	0.654	0.731	0.577	0.633	0.682
PTR_{8mm}	0.496 (0.3315–0.6596)	0.481	0.500	0.462	0.481	0.480
Clinical	0.607 (0.4466–0.7679)	0.654	0.885	0.423	0.605	0.786
Nomogram	0.889 (0.7987–0.9794)	0.846	0.769	0.923	0.909	0.800

AUC: area under the curve; *CI*: confidence interval; *PPV*: positive predictive value; *NPV*: negative predictive value

cohort was 0.889 (95%CI: 0.799–0.979). As illustrated in Fig. 6C, Delong tests demonstrated that the developed nomogram ($p = 0.002$) and TR-PTR_{2mm} model ($p = 0.039$) outperformed the clinical model in prognosis prediction for HCC. However, no significant difference was found in prediction performance between the constructed nomogram and TR-PTR_{2mm} model ($p = 0.127$). The calibration curves of these three models were displayed in Fig. 6D, and the Hosmer-Lemeshow test confirmed a superiority of the nomogram on the alignment of predicted probability and actual probability (nomogram: $p > 0.05$). The DCA curves (Fig. 6E) indicated that the net benefit in prognosis prediction by using the developed nomogram was enhanced compared to that by using clinical model alone or TR-PTR_{2mm} model alone, suggesting a potential of the developed nomogram in clinical application.

Discussion

This study aimed to comprehensively evaluate the power of intra- and peritumoral radiomics based on ^{18}F-FDG PET/CT images in predicting prognosis for HCC. As indicated, the TR-PTR_{2mm} radiomic model was identified as the optimal model to predict prognosis. Furthermore, the AUC of a nomogram combining the TR-PTR_{2mm}

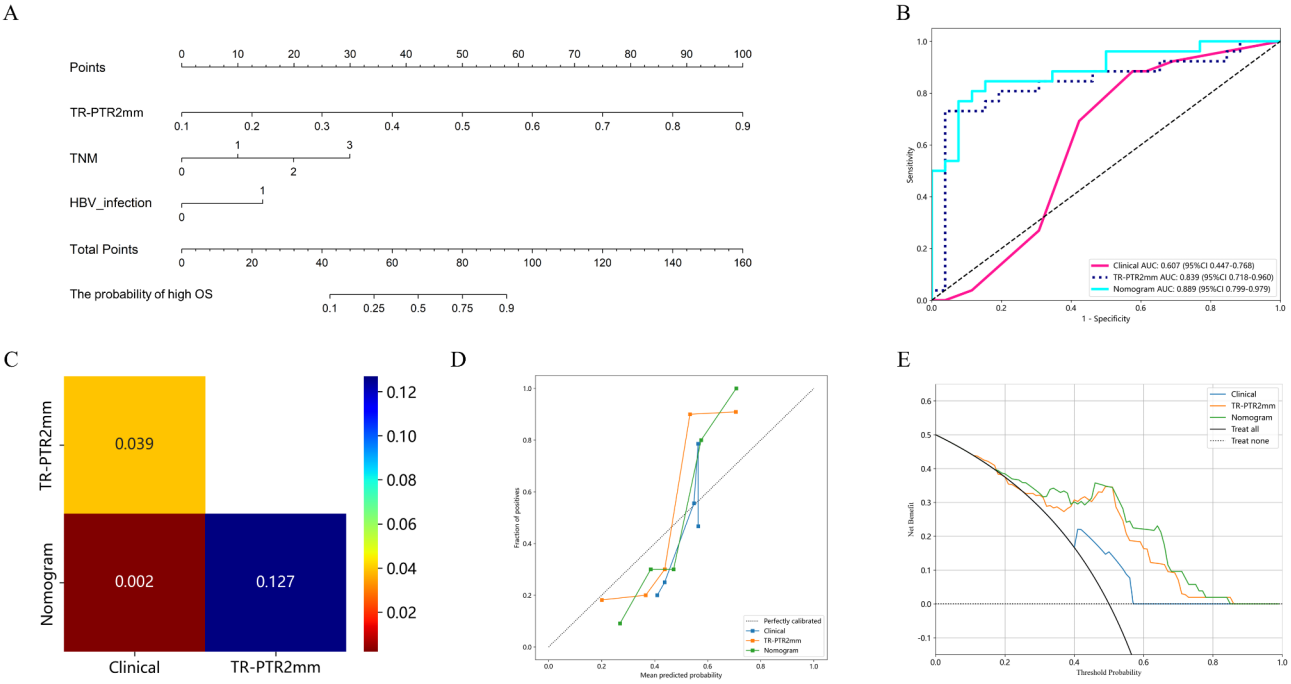

Fig. 6 The construction and performance of the nomogram. (**A**) The developed nomogram incorporating the TR-PTR$_{2mm}$ model with two independent clinical predictors in the differentiating Low OS group from High OS group for HCC. (**B**) ROC curves of the TR-PTR$_{2-8\,mm}$ model, Clinical model were drawn. The nomogram with an AUC of 0.889 (95%CI 0.799–0.979) outperformed the other two models in the external validation cohort. (**C**) As illustrated, Delong tests demonstrated that the developed nomogram ($p = 0.002$) and TR-PTR$_{2mm}$ model ($p = 0.039$) outperformed the clinical model in prognosis prediction for HCC. Whereas, no significant difference was found between the constructed nomogram and TR-PTR$_{2mm}$ model ($p = 0.127$). (**D**) As indicated in the calibration curves, the nomogram exhibited a superiority on the alignment of predicted probability and actual probability (nomogram: Hosmer-Lemeshow test, $p > 0.05$). (**E**) The DCA curves also confirmed the outperformance of the nomogram over the other two models in the net benefit

model with significant clinical characteristics was further elevated to 0.889, suggesting a potential application in clinical practice.

Though microvascular invasion (MVI) stands as a crucial prognostic factor for HCC amongst a variety of histopathological characteristics, it is a histologic finding exclusively obtained postoperatively based on histopathological analysis of resected specimens but not biopsy, thus increasing radiomic studies are being conducted to predict MVI in HCC [32–34]. Since the ultimate purpose of predicting MVI was to indicate prognosis, machine learning models constructed to directly predict OS would be acceptable. At present, machine learning and radiomic models are emerging as promising tools for prognosis prediction [6, 8, 35]. However, the majority of radiomics were based on CT and/or MRI images, and the PET/CT derived radiomics was rare for HCC. Previous study from Shi et al., evaluated the potential of texture features and metabolic parameters based on ^{18}F-FDG PET images in predicting the status of MVI in HCC [36]. In our study, none of the traditional PET metabolic parameters (SUVmax, SUVmean, SUVpeak, SUL, MTV, TLG and TMR) were able to distinguish Low OS group from High OS group ($p > 0.05$). Given these metabolic parameters are generalized metrics that ignored the heterogeneity in tumor, a high throughput of radiomic features extracted based on VOI segmentation and subsequently constructed radiomic models are expected to exhibit superiority in characterization of heterogeneity and prognosis prediction.

The peritumoral region, where the tumor cells interact with the surrounding normal tissue cells, constitutes the external microenvironment of the tumor [37, 38]. With the tumor development and progression, the tumor infiltration into adjacent normal tissues result in morphological and textural alterations in the surrounding area. Presumably, the peritumoral region harbors valuable information regarding tumor invasiveness and prognosis[39, 40]. Consistently, the role of peritumoral radiomics in clinical practice for HCC is constantly underscored. Shan et al. constructed peritumoral radiomics signatures based on peritumoral (2 mm) VOI to predict early recurrence of HCC [40]. As reported, the peritumoral radiomic model based on CT images outperformed the traditional intratumoral radiomic model. Chen et al. developed a combined intratumoral and peritumoral radiomics model based on MRI images for prediction of immuno-score (0–2 vs. 3–4) in HCC [39]. The combined intratumoral and peritumoral region was generated by dilating the intratumoral region at a radius

of 1 cm. Regarding to the optimal peritumoral region size, a comprehensive study involving multiple patterns of peritumoral region is needed. Zhang et al. developed two peritumoral models creating by additional 2 mm and 5 mm peritumoral areas from tumoral region based on MRI images, to predict RFS of HCC patients after surgical resection [35]. The results demonstrated that no significant difference was observed in the prediction performance between the two peritumoral radiomic models. As reported in a study from Zhao et al., a total of three integrated intratumoral and peritumoral radiomic models based on intratumoral region and peritumoral region (3 mm, 5 mm, and 10 mm) from contrast-enhanced MRI images were constructed to predict response to transcatheter arterial chemoembolization (TACE) treatment in HCC [7]. Among them, the intratumoral and peritumoral (3 mm) radiomic model was proved to be the optimal model with an AUC of 0.911 (95%CI, 0.825–0.975). The divergence in the determination of the optimal peritumoral region size need to be resolved in consensus.

In the present investigation, a systematic exploration of the optimal peritumoral size was conducted to identify the optimal PET/CT derived radiomic model in prognosis prediction for HCC. In our study, peritumoral radiomic models were constructed based on multiple patterns of peritumoral regions with varying thicknesses, including 2 mm, 4 mm, 6 mm and 8 mm. Except for intratumoral radiomics alone and peritumoral radiomics alone, integrated intratumoral and peritumoral radiomic models were also developed. As indicated in the results, the $PTR_{2-8\ mm}$ models alone were not able to predict prognosis for HCC, whereas the PTR could provide significantly supplementary information to enhance the prediction efficacy of the TR-$PTR_{2-8\ mm}$ radiomic models. Additionally, the performance of TR-$PTR_{2-8\ mm}$ model was alleviated with increasing peritumoral radius, manifesting that the internal and 2 mm-external microenvironment of the tumor was able to provide sufficient and valuable prognostic information. Further biological validation is needed to provide reasonable explanation for the role of TR-PTR_{2mm} radiomic model in prognosis prediction for HCC.

Several limitations should be addressed in the study. First, this radiomic analysis is retrospective in nature, though both an internal validation and an independent external validation from two centers were included in the present investigation. A prospective study with a large sample size from multiple institutions is warranted in near future. Second, the included HCC patients from the two institutions underwent PET/CT examinations by using two distinct scanning devices, which would inevitably cause potential bias in the results. To mitigate this issue, Combat harmonization was employed in the process of images pre-processing before radiomic analysis. Then, no subgroup radiomics was performed based on stratification for HCC patients in the study. A further study with a sufficient sample size is expected to elaborate this issue. In the end, though a comprehensive radiomic analysis involving intratumoral regions and peritumoral regions was conducted, no habitat radiomics based on segmentations of functional subregions for HCC was included in the study, which is exactly what we aim to do in our future study.

Conclusion

In summary, a comprehensive radiomic analysis involving segmentation of intratumoral and/or peritumoral VOI based on ^{18}F-FDG PET/CT images was conducted to identify an optimal radiomic model in prognosis prediction for HCC. The integrated radiomic model based on a combination of intratumoral region with a 2 mm peripheral region was proved to be the optimal model, suggesting a supplementary role of peritumoral radiomics in predicting survival for HCC, especially for a peritumoral region within a 2 mm thickness to the tumor boundary. Additionally, a nomogram incorporating this integrated intratumoral and peritumoral radiomic model with informative clinical indicators exhibited a further improved performance in prognosis prediction for HCC, which is potentially applied in clinical practice.

Abbreviations

AUC	Area under the curve
BCLC	Barcelona Clinic Liver Cancer staging system
CLIP	Cancer of the Liver Italian Program
CT	Computed tomography
DCA	Decision curve analysis
DFS	Disease free survival
^{18}F-FDG PET/CT	^{18}F-Fluorodeoxyglucose positron emission tomography/computed tomography
HCC	Hepatocellular carcinoma
LASSO	Least absolute shrinkage selection operator
LightGBM	Light Gradient Boosting Machine
LR	Logistic Regression
MLP	Multilayer Perceptron
MRI	Magnetic resonance imaging
MTV	Metabolic tumor volume
MVI	Microvascular invasion
NB	NaiveBayes
NPV	Negative predictive value
OS	Overall survival
PPV	Positive predictive value
RFS	Recurrence free survival
ROC	Receiver operator characteristic
SUL	SUV normalized to lean body mass
SUV	Standardized uptake value
SVM	Support vector machine
TACE	Transcatheter arterial chemoembolization
TLG	Total lesion glycolysis
TLR	Tumor liver uptake ratio
TMR	Tumor to mediastinum ratio
VOI	Volume of interest

Supplementary Information

The online version contains supplementary material available at https://doi.org/10.1186/s12885-025-13649-4.

Supplementary Material 1

Acknowledgements
We really appreciated the support from the colleagues and staff in our department of our institution during the study. Additionally, we are grateful for the technical assistance provided by the OnekeyAI platform.

Author contributions
CS analysed the data and drafted the original manuscript. KC analysed the data. ED, RT and YL collected the data. XL, WX and JS reviewed the manuscript.

Funding
This work was supported by grants from the National Natural Science Foundation of China (82272074), Tianjin Health Science and Technology Project (TJWJ2021MS013), and Tianjin Key Medical Discipline (Specialty) Construction Project (TJYXZDXK-009A).

Data availability
The raw data is not publicly available due to the privacy protection for all the patients enrolled in the study, which is only available from the corresponding authors on reasonable requests.

Declarations

Ethics approval and consent to participate
This retrospective study was approved by the Institutional Ethics Committee of Tianjin Medical University Cancer Hospital (EK20240068), and was conducted following the principles outlined in the Declaration of Helsinki and other relevant ethical guidelines. The requirement for informed consent was waived by the Ethics Committee of Tianjin Medical University Cancer Hospital because of the retrospective nature of the study.

Consent for publication
Not applicable.

Competing interests
The authors declare no competing interests.

Conflict of interest
All authors declared that they have no conflicts of interest.

Author details
[1]Department of Molecular Imaging and Nuclear Medicine, Tianjin Medical University Cancer Institute and Hospital, Tianjin 300060, China
[2]Key Laboratory of Cancer Prevention and Therapy, National Clinical Research Center for Cancer, Tianjin's Clinical Research Center for Cancer, Tianjin 300060, China
[3]Hangzhou Institute of Medicine (HIM), Zhejiang Cancer Hospital, Chinese Academy of Sciences, Hangzhou, Zhejiang 310022, China
[4]Department of Nuclear Medicine, Tianjin First Central Hospital, Tianjin 300192, China
[5]Department of Neurosurgery, Shandong Provincial Hospital Affiliated to Shandong First Medical University, Jinan, Shandong 250021, China

Received: 18 June 2024 / Accepted: 5 February 2025
Published online: 19 February 2025

References

1. Siegel RL, Miller KD, Wagle NS, Jemal A. Cancer statistics, 2023. CA Cancer J Clin. 2023;73:17–48.
2. Lee SM, Kim HS, Lee S, Lee JW. Emerging role of (18)F-fluorodeoxyglucose positron emission tomography for guiding management of hepatocellular carcinoma. World J Gastroenterol. 2019;25:1289–306.
3. Wang Q, Li C, Zhang J, et al. Radiomics models for predicting microvascular invasion in hepatocellular carcinoma: a systematic review and radiomics quality score assessment. Cancers (Basel). 2021;13(22):5864.
4. Wakabayashi T, Ouhmich F, Gonzalez-Cabrera C, et al. Radiomics in hepatocellular carcinoma: a quantitative review. Hep Intl. 2019;13:546–59.
5. Lai Q, Spoletini G, Mennini G, et al. Prognostic role of artificial intelligence among patients with hepatocellular cancer: a systematic review. World J Gastroenterol. 2020;26:6679–88.
6. Cannella R, Santinha J, Bèaufrere A, et al. Performances and variability of CT radiomics for the prediction of microvascular invasion and survival in patients with HCC: a matter of chance or standardisation? Eur Radiol. 2023;33:7618–28.
7. Zhao Y, Zhang J, Wang N, et al. Intratumoral and peritumoral radiomics based on contrast-enhanced MRI for preoperatively predicting treatment response of transarterial chemoembolization in hepatocellular carcinoma. BMC Cancer. 2023;23(1):1026.
8. Li N, Wan X, Zhang H, Zhang Z, Guo Y, Hong D. Tumor and peritumor radiomics analysis based on contrast-enhanced CT for predicting early and late recurrence of hepatocellular carcinoma after liver resection. BMC Cancer. 2022;22:664.
9. Xu X, Zhang H-L, Liu Q-P, et al. Radiomic analysis of contrast-enhanced CT predicts microvascular invasion and outcome in hepatocellular carcinoma. J Hepatol. 2019;70:1133–44.
10. Leger MA, Routy B, Juneau D. FDG PET/CT for Evaluation of Immunotherapy Response in Lung Cancer patients. Semin Nucl Med. 2022;52:707–19.
11. Jiang C, Zhao L, Xin B, Ma G, Wang X, Song S. (18)F-FDG PET/CT radiomic analysis for classifying and predicting microvascular invasion in hepatocellular carcinoma and intrahepatic cholangiocarcinoma. Quant Imaging Med Surg. 2022;12:4135–50.
12. Fiz F, Masci C, Costa G, et al. PET/CT-based radiomics of mass-forming intrahepatic cholangiocarcinoma improves prediction of pathology data and survival. Eur J Nucl Med Mol Imaging. 2022;49:3387–400.
13. Li Y, Zhang Y, Fang Q, et al. Radiomics analysis of [(18)F]FDG PET/CT for microvascular invasion and prognosis prediction in very-early- and early-stage hepatocellular carcinoma. Eur J Nucl Med Mol Imaging. 2021;48:2599–614.
14. Han JH. Evaluation of prognostic factors on recurrence after curative resections for hepatocellular carcinoma. World J Gastroenterol. 2014;20(45):17132–640.
15. Cho KJ, Choi NK, Shin MH, Chong AR. Clinical usefulness of FDG-PET in patients with hepatocellular carcinoma undergoing surgical resection. Annals of Hepato-Biliary-Pancreatic Surgery 21; 2017.
16. Wei J, Jiang H, Gu D, et al. Radiomics in liver diseases: current progress and future opportunities. Liver Int. 2020;40:2050–63.
17. Napel S, Mu W, Jardim-Perassi BV, Aerts H, Gillies RJ. Quantitative imaging of cancer in the postgenomic era: radio(geno)mics, deep learning, and habitats. Cancer. 2018;124:4633–49.
18. Zhang L, Wang Y, Peng Z, et al. The progress of multimodal imaging combination and subregion based radiomics research of cancers. Int J Biol Sci. 2022;18:3458–69.
19. Khodabakhshi Z, Amini M, Mostafaei S, et al. Overall Survival Prediction in Renal Cell Carcinoma patients using computed Tomography Radiomic and Clinical Information. J Digit Imaging. 2021;34:1086–98.
20. Wakabayashi T, Ouhmich F, Gonzalez-Cabrera C, et al. Radiomics in hepatocellular carcinoma: a quantitative review. Hepatol Int. 2019;13:546–59.
21. Yin X, Liao H, Yun H, et al. Artificial intelligence-based prediction of clinical outcome in immunotherapy and targeted therapy of lung cancer. Semin Cancer Biol. 2022;86:146–59.
22. Wei J, Ji Q, Gao Y, et al. A multi-scale, multi-region and attention mechanism-based deep learning framework for prediction of grading in hepatocellular carcinoma. Med Phys. 2022;50:2290–302.
23. Zhang L, Cai P, Hou J, Luo M, Li Y, Jiang X. Radiomics Model based on Gadoxetic Acid Disodium-enhanced MR Imaging to Predict Hepatocellular Carcinoma Recurrence after curative ablation. Cancer Manage Res Volume. 2021;13:2785–96.
24. Shi J, Dong Y, Jiang W, et al. MRI-based peritumoral radiomics analysis for preoperative prediction of lymph node metastasis in early-stage cervical cancer: a multi-center study. Magn Reson Imaging. 2022;88:1–8.
25. Kim S, Shin J, Kim D-Y, Choi GH, Kim M-J, Choi J-Y. Radiomics on Gadoxetic acid–enhanced magnetic resonance imaging for prediction of postoperative early and late recurrence of single Hepatocellular Carcinoma. Clin Cancer Res. 2019;25:3847–55.
26. Sala E, Mema E, Himoto Y, et al. Unravelling tumour heterogeneity using next-generation imaging: radiomics, radiogenomics, and habitat imaging. Clin Radiol. 2017;72:3–10.

27. Tian Y, Hua H, Peng Q, et al. Preoperative evaluation of Gd-EOB-DTPA-Enhanced MRI Radiomics-based Nomogram in Small Solitary Hepatocellular Carcinoma (=3 cm) with Microvascular Invasion: a two-Center Study</at. J Magn Reson Imaging. 2022;56:1459–72.
28. Chong H, Gong Y, Pan X, et al. Peritumoral Dilation Radiomics of Gadoxetate Disodium-enhanced MRI excellently predicts early recurrence of Hepatocellular Carcinoma without Macrovascular Invasion after Hepatectomy. J Hepatocellular Carcinoma Volume. 2021;8:545–63.
29. Fiz F, Rossi N, Langella S, et al. Radiomic analysis of intrahepatic cholangiocarcinoma: non-invasive prediction of pathology data: a multicenter study to develop a clinical–radiomic model. Cancers (Basel). 2023;15(17):4204.
30. Chen K, Wang J, Li S, Zhou W, Xu W. Predictive value of 18F-FDG PET/CT-based radiomics model for neoadjuvant chemotherapy efficacy in breast cancer: a multi-scanner/center study with external validation. Eur J Nucl Med Mol Imaging. 2023;50:1869–80.
31. Chen Y, Wang Z, Yin G, et al. Prediction of HER2 expression in breast cancer by combining PET/CT radiomic analysis and machine learning. Ann Nucl Med. 2022;36:172–82.
32. Chen Y-D, Zhang L, Zhou Z-P, et al. Radiomics and nomogram of magnetic resonance imaging for preoperative prediction of microvascular invasion in small hepatocellular carcinoma. World J Gastroenterol. 2022;28:4399–416.
33. Zhang K, Zhang L, Li W-C, et al. Radiomics nomogram for the prediction of microvascular invasion of HCC and patients' benefit from postoperative adjuvant TACE: a multi-center study. Eur Radiol. 2023;33:8936–47.
34. Wang Y, Luo S, Jin G, Fu R, Yu Z, Zhang J. Preoperative clinical-radiomics nomogram for microvascular invasion prediction in hepatocellular carcinoma using [Formula: see text]F-FDG PET/CT. BMC Med Imaging. 2022;22:70.
35. Zhang L, Hu J, Hou J, Jiang X, Guo L, Tian L. Radiomics-based model using gadoxetic acid disodium-enhanced MR images: associations with recurrence-free survival of patients with hepatocellular carcinoma treated by surgical resection. Abdom Radiol. 2021;46:3845–54.
36. Shi H, Duan Y, Shi J et al. Role of preoperative prediction of microvascular invasion in hepatocellular carcinoma based on the texture of FDG PET image: a comparison of quantitative metabolic parameters and MRI. Front Physiol. 2022;13:928969.
37. Ding J, Chen S, Serrano Sosa M, et al. Optimizing the Peritumoral Region Size in Radiomics Analysis for Sentinel Lymph Node Status prediction in breast Cancer. Acad Radiol. 2022;29(Suppl 1):S223–8.
38. Li Y, Ammari S, Lawrance L, et al. Radiomics-based method for predicting the glioma subtype as defined by tumor grade, IDH mutation, and 1p/19q codeletion. Cancers (Basel). 2022;14(7):1778.
39. Chen S, Feng S, Wei J, et al. Pretreatment prediction of immunoscore in hepatocellular cancer: a radiomics-based clinical model based on Gd-EOB-DTPA-enhanced MRI imaging. Eur Radiol. 2019;29:4177–87.
40. Shan Q-y, Hu H-t, Feng S-t, et al. CT-based peritumoral radiomics signatures to predict early recurrence in hepatocellular carcinoma after curative tumor resection or ablation. Cancer Imaging. 2019;19(1):11.

Publisher's note

Springer Nature remains neutral with regard to jurisdictional claims in published maps and institutional affiliations.